CCM-80-5

Center for Composite Materials

CHARACTERIZATION OF THE
INTERLAMINAR SHEAR FATIGUE PROPERTIES
OF SMC R-50*

DALE W. WILSON

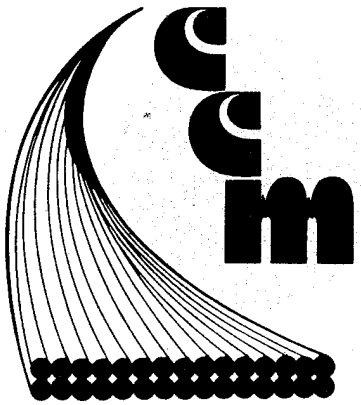

College of Engineering
University of Delaware
Newark, Delaware

CHARACTERIZATION OF THE INTERLAMINAR SHEAR FATIGUE PROPERTIES OF SMC R-50*

by

Dale W. Wilson

Center for Composite Materials
Department of Mechanical and Aerospace Engineering
University of Delaware
Newark, Delaware 19711

May 1980

ABSTRACT

The interlaminar shear fatigue behavior of the sheet molding compound SMC-R50* has been studied. A thick-laminate short beam shear test was employed to characterize S-N behavior for the material at 21°C and 90°C. The shear modulus (G_{xz}) was determined at 21°C and 90°C and the effect of fatigue on modulus at both test temperatures is discussed. SEM and optical photomicrographs of untested and fatigued specimens were studied to assess the relationship between material microstructure and the observed fatigue results for strength and modulus. The experimental evidence suggests that the fatigue life for this material is determined by a flow criticality failure mechanism, not cumulative damage.

*Owens Corning Fiberglas

INTRODUCTION

Light weight combined with excellent strength and stiffness properties have made advanced composites a prime candidate for many weight-critical structural applications. Recently the composites technology has shifted from strictly high technology, low volume aerospace applications to the large volume automotive and industrial marketplaces. Large volume production has shifted material emphasis to chopped fiber sheet molding compounds (SMC) because of the cost and processing advantages.

In all composite systems the secondary properties often become design-critical parameters. Interlaminar properties which resist the σ_z , τ_{xz} and τ_{yz} interlaminar stresses are the weakest link in the system. Interlaminar strength is controlled by matrix and fiber-matrix interface properties which are often several orders of magnitude less than the strength of the fibers. This inherent weakness of the matrix phase is compounded by environmental and fatigue sensitivity which can result in further degradation of the interlaminar properties.

Despite the importance of the interlaminar properties little work in characterizing them has been done for the

plethora of materials in use today. This is due to the difficulty of experimentally characterizing interlaminar properties. The most widely used method for determination of interlaminar shear strength (ILS) is the short beam shear test (ASTM D2344-76).

Economics is the driving force behind the widespread usage of the short beam shear test, not the accuracy of the results. Several studies have focused upon assessing the validity of test results using the short beam shear test. Kellog and Sattar [1] and later Kedward [2] published works on the effects of test coupon geometry and anisotropy on the shear stress distributions and failure mode/strength in composites. If properly designed, the short beam shear test can provide test data sufficiently accurate to use as a comparative data base. This makes it a viable test method to use in the study of temperature and fatigue effects on ILS strength.

A scaled-up version of the short beam shear specimen was used by Pipes [3] to measure ILS modulus and strength for unidirectional boron epoxy, graphite epoxy and glass epoxy materials. The stress distribution in this thick specimen was analyzed using photoelasticity and finite element methods. In later work Pipes [4] characterized the fatigue behavior in unidirectional laminates of the

same three materials using the thick-laminate short beam shear test method. The results indicate that ILS strength degrades much faster in fatigue than the axial properties. Works by Owen and Morris [5], Dharin [6] and Bevan [7] report similar findings for orthogonally cross-plied and unidirectional laminates of carbon fiber-reinforced plastic (CRFP). These works also investigated the effects of sizing agents, thermal aging and fiber volume fraction respectively on ILS strengths both statically and in fatigue. In summary, all of these results emphasize the sensitivity of the interlaminar properties to fatigue damage. Microstructural analysis [8,9] reveals that matrix crazing and fiber-matrix disbonding are the primary forms of damage resulting from fatigue. This type of damage in turn results in the degradation of the critically low interlaminar properties.

All of the studies reported in the literature have dealt with continuous fiber composites. In this study the ILS behavior of a short fiber SMC was evaluated. The S-N behavior was characterized at ambient and 90°C temperatures using the thick-laminate short beam shear test method. This enabled the measurement of modulus data at various points on the S-N curve which when coupled with SEM studies provided knowledge about the failure mechanism.

EXPERIMENTAL METHOD

The characterization of fatigue effects on strength and modulus in SMC-R50 was accomplished using the thick-laminate short beam shear test developed by Pipes [3]. Initially static tests were used to verify the test technique and provide baseline data for the fatigue studies. Specimens were subjected to sinusoidal loadings over a spectrum of stress levels to develop fatigue life (S-N) curves at 21°C and 90°C. Modulus measurements and scanning electron microscopy (SEM) were used to analyze the failure mechanism.

Specimen Fabrication

The thick-laminate short beam shear test requires approximately a 12.5 mm (0.5 in) thick specimen in order to accommodate the strain instrumentation for determination of the shear modulus, G_{xy}. The greatest thickness of SMC-R50 which could be obtained was 9.53 mm (0.375 in). This panel thickness in combination with the material properties resulted in the necessity to develop a sandwich construction specimen of the geometry shown in Figure 1. The faces were unidirectional AS/3501-6 graphite/epoxy bonded to the SMC with American Cyanimide FM300 adhesive. The specimen size

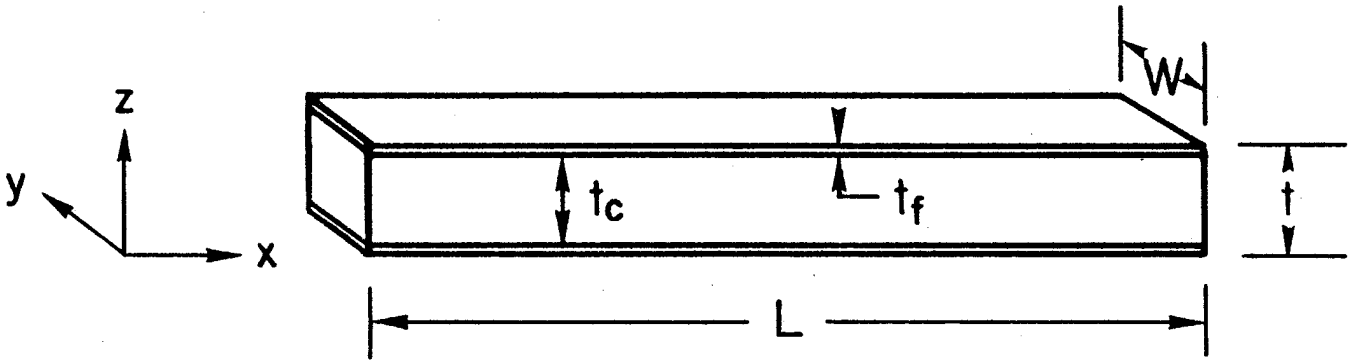

$L = 3.0$ in

$t = 0.450$ in

$W = 0.375$ in

$t_c = 0.325$ in

$t_f = 0.063$ in

Figure 1. Specimen geometry and typical dimensions

was 76 mm (3.0 in) in length x 95 mm (.375 in) in width x 12.5 mm (.5 in) in thickness. Trial tests were used to experimentally verify that the proper shear failure mode was achieved. Although the SMC should be random in plane and exhibit planar isotropy, some preferential fiber orientation is often found making the actual properties orthotropic. In accordance with this observation all specimens were cut from the panel in a single direction with a diamond wafing saw to eliminate fiber orientation as a variable.

Test Apparatus

A special fixture, depicted in Figure 2, was developed to apply the three-point bending loads to the specimen. To minimize stress concentrations, 6.3 mm (0.25-inch) width flat reaction pads were fabricated from copper sheet. The outer two reaction pads were designed to pivot to allow for specimen bending deformation during test. This fixture was mounted inside an environmental chamber and to the load frame of an Instron Model 1321 Servo-Hydraulic machine.

Tests were carried out under load control at a frequency of 5 Hz. The ratio of minimum to maximum stress amplitude (R) was equal to a constant of 0.1 over the range of stress levels investigated. A minimum of five specimens were tested at each stress level. The number of cycles to failure were recorded for all fatigue

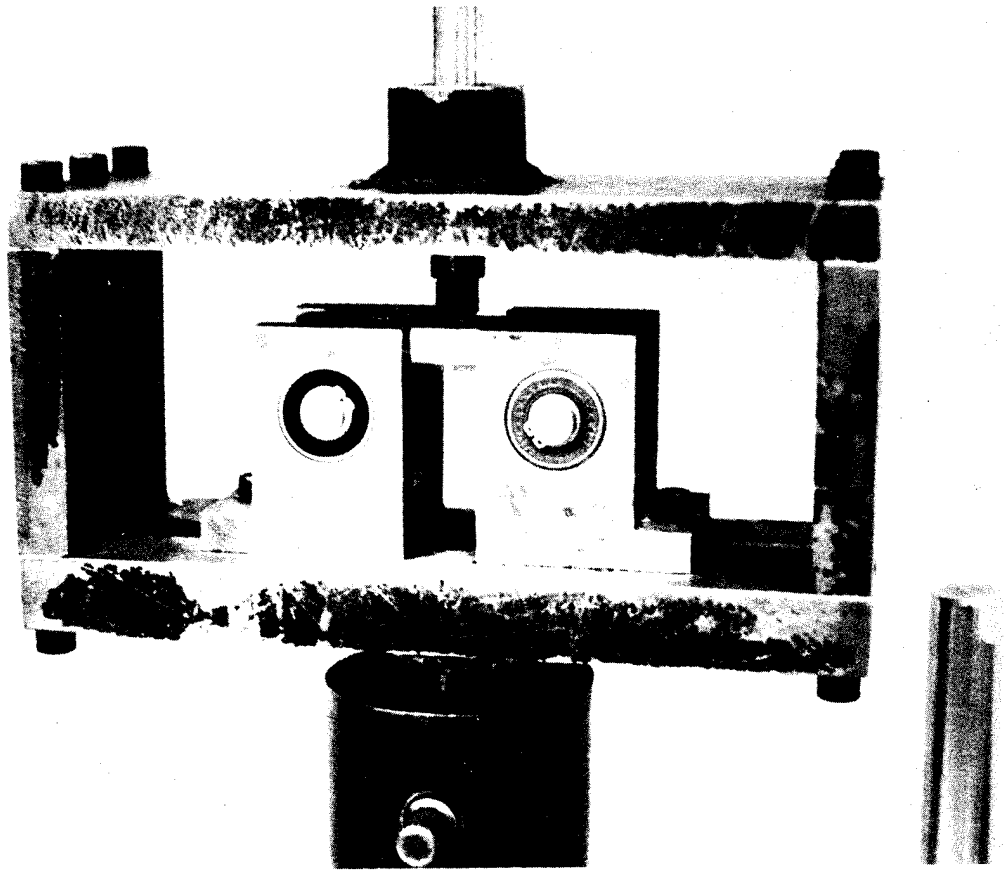

Figure 2. Test fixture for the three point bending load application

failures and specimens which did not fail in fatigue after 10^6 cycles were tested statically for residual strength.

Shear Modulus Measurement

Measurement of the interlaminar shear modulus (G_{xz}) is complicated by the nonuniform distribution of the shearing stress along the length of the beam. A finite-element analysis of the test geometry revealed well behaved shear stress distributions at the quarter span. This region of uniform stress was chosen as the site for strain measurement. While computing the exact stresses at the quarter span for each load is possible using the finite element analysis, approximate representation of the stresses predicted by Euler beam theory at the beam quarter span is satisfactory for comparative studies.

Strains were measured using stacked, strain rosettes with (1.52 mm) (0.06 in) grids. The rosettes were placed on the neutral axis and at the quarter span as shown in Figure 3. After careful positioning and alignment in the test fixture, the specimens were loaded and strains measured at 98 N increments to approximately one-half the average ultimate shear strength of the material. Modulus was determined for unfatigued specimens at 21°C and 90°C to serve as control data. Measurements

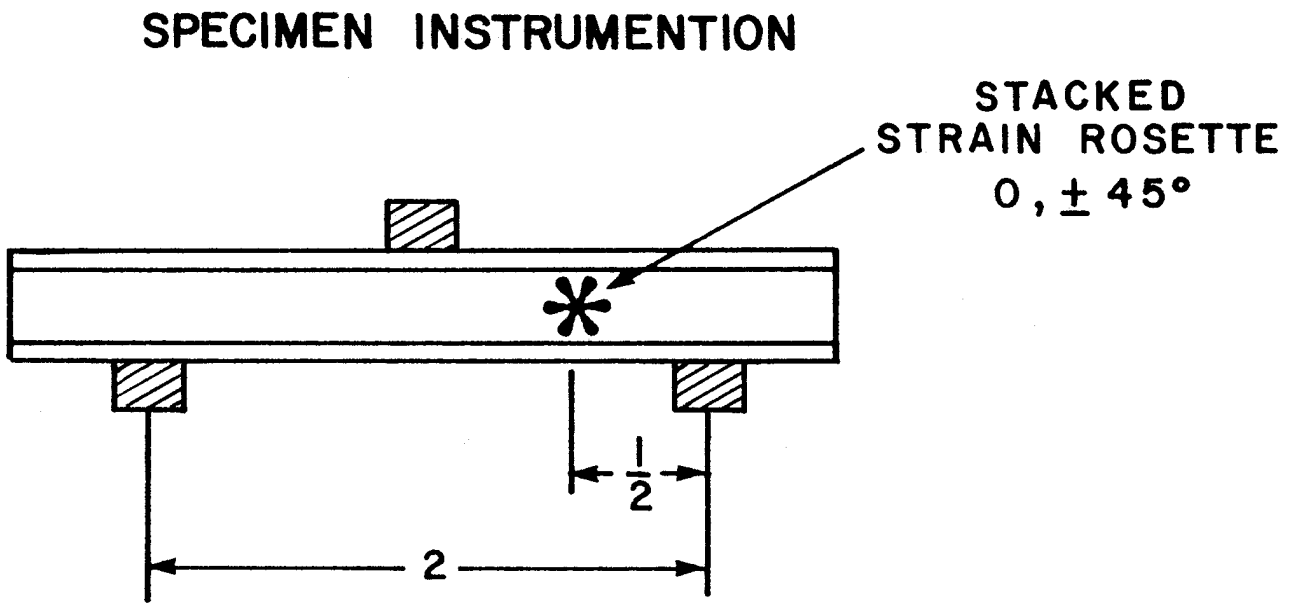

Figure 3. Strain rosette location for Modulus measurement

were then made on specimens tested to varying percentages of their fatigue life.

Microstructural Studies

Microstructural damage in specimens subjected to fatigue loading was examined using a Phillips PSEM 501 scanning electron microscope. Cross sections were removed from the quarter span region of an untested control and failed for each S level and test temperature. The samples were prepared using standard polishing procedures and then the surfaces were gold coated by sputtering. A thorough inspection of each specimen was made at a 320X magnification and details were examined by using 640X magnification.

Flexural Strength Tests

The thickness of the SMC-R50 panel used in fabrication of the test specimens invoked concern over the uniformity of material properties through the thickness. Exothermic reactions take place during curing of thick sections which could lead to a difference between properties along the midplane and outer surfaces. Twenty-six samples were sectioned lengthwise to produce flexure bars with material from the center region on one of the surfaces. Half of the specimens were tested in flexure with material from the center region in tension and the other half with

the outer surface material in tension. Any significant difference in the material properties would result in a difference in flexural strength.

RESULTS AND DISCUSSION

Static Interlaminar Shear Strength

The static test results reported in Tables 1 and 2 form the data base to be used for comparison of the fatigue data. The mean ILS strength for the SMC-R50 at 21°C computed from Table 1 was 29.5 MPa (4281 psi) with a standard deviation of 2.5 MPa (±364 psi). At 90°C the mean ILS strength decreased to 23.2 MPa (3364 psi) with a standard deviation of 0.72 MPa (±105 psi). These ILS strengths were computed from standard Euler beam theory.

Flexural Strength Results

Results from the flexural strength tests were designed to evaluate the through-the-thickness material properties are shown in Table 3. The mean flexural strengths for the inside and outside regions were 233.1 MPa (3.381×10^4 psi) and 256.6 MPA (3.721×10^4 psi) respectively. Statistical analysis revealed that for the number of samples tested, within 95% confidence limits, the strengths for the two regions are not significantly different. Therefore, the flexural material properties appear to be uniform through the thickness.

Fatigue Life Characterization

The fatigue life behavior of SMC-R50 is summarized in Figures 4 and 5 for the 21°C and 90°C test temperatures.

TABLE 1

STATIC ILS STRENGTH OF SMC-R50 at 21°C

Specimen	Width (mm)	Thick (mm)	Load (kg)	Span (mm)	Strength (MPa)
2C-2	9.3	12.3	409	50.8	26.2
2C-4	9.7	12.3	562	50.8	32.4
2C-5	9.4	12.4	510	50.8	32.5
2C-6	9.6	12.3	470	50.8	29.3
2C-7	8.6	12.3	385	50.8	27.0
4B-1	8.2	11.4	380	50.8	30.0
4B-11	9.6	11.6	445	50.8	29.6

TABLE 2

STATIC ILS STRENGTHS OF SMC-R50 AT 90°C

Specimen	Width (mm)	Thick (mm)	Load (kg)	Span (mm)	Strength (MPa)
2B-2	9.53	12.73	390	50.8	23.7
2B-3	9.55	12.70	385	50.8	23.4
2B-5	9.55	12.70	390	50.8	23.7
2B-6	9.58	12.67	385	50.8	23.3
2B-7	9.58	12.62	360	50.8	21.9

TABLE 3

FLEXURAL STRENGTH RESULTS

Specimen	Width (mm)	Thickness (mm)	Load (N)	Span (mm)	Edge Being Tested	Strength (MPa)
5A-1-2	9.45	2.87	271	50.8	inside	269.0
5A-2-2	9.50	3.73	351	50.8	inside	203.3
5A-4-1	9.55	3.40	343	50.8	inside	236.6
5A-4-2	9.55	3.71	481	50.8	inside	279.0
5A-5-1	9.58	3.43	363	50.8	inside	245.7
5A-5-2	9.58	3.73	538	50.8	inside	308.1
5A-6-1	9.63	3.71	401	50.8	inside	231.6
5A-7-1	9.65	3.58	401	50.8	inside	247.6
5A-9-2	9.80	3.33	412	50.8	inside	289.3
5A-10-1	9.30	3.73	471	50.8	inside	277.0
5A-11-1	9.47	3.76	383	50.8	inside	214.9
5A-12-1	9.47	351	334	50.8	inside	216.3
5A-13-1	9.68	3.61	432	50.8	inside	261.3
5A-1-1	9.42	4.39	599	50.8	outside	250.6
5A-2-1	9.50	3.73	461	50.8	outside	193.1
5A-3-1	9.55	3.58	392	50.8	outside	244.2
5A-3-2	9.55	3.66	432	50.8	outside	257.6
5A-6-2	9.60	3.45	441	50.8	outside	293.7
5A-7-2	9.65	3.56	452	50.8	outside	281.8
5A-8-1	9.65	3.71	353	50.8	outside	202.8
5A-8-2	9.68	3.51	461	50.8	outside	295.6
5A-9-1	9.80	3.78	441	50.8	outside	239.6
5A-10-2	9.30	3.40	392	50.8	outside	277.7
5A-11-2	9.5	3.35	403	50.8	outside	330.6
5A-12-2	9.5	3.63	422	50.8	outside	256.5
5A-13-1	9.65	3.58	343	50.8	outside	211.4

The data is presented as S-N fatigue life curves for specimens cycles at a constant stress amplitude ratio of 0.1 (R=0.1). In Figure 4 the S-N behavior of SMC-R50 at room temperature shows that the endurance limit extrapolates to approximately 62 percent of the ultimate shear strength. At 10^6 cycles the fatigue strength approaches approximately 64 percent of the static ultimate shear strength. The specimens tested at the 53% and 44% levels ran out at 10^6 cycles. Residual strength tests revealed that after 10^6 cycles in fatigue at these two S levels the average shear strength was 96 percent of the average static ultimate.

A similar S-N representation of the fatigue behavior of SMC-R50 at 90°C is shown in Figure 5. The large amount of scatter in data prohibits accurate extrapolation to determine an endurance limit. The endurance limit is greater than 45% of the average static ultimate strength but less than 50%. At 90°C the strength degradation is more rapid and more severe than at R.T. Samples tested at the 45 percent S level endured 10^6 cycles and were tested for residual strength. The average residual strength of these specimens was 80% of the average static ultimate shear strength. The significance of the residual strength measurements becomes apparent when considered in connection with modulus data and microstructural studies discussed later.

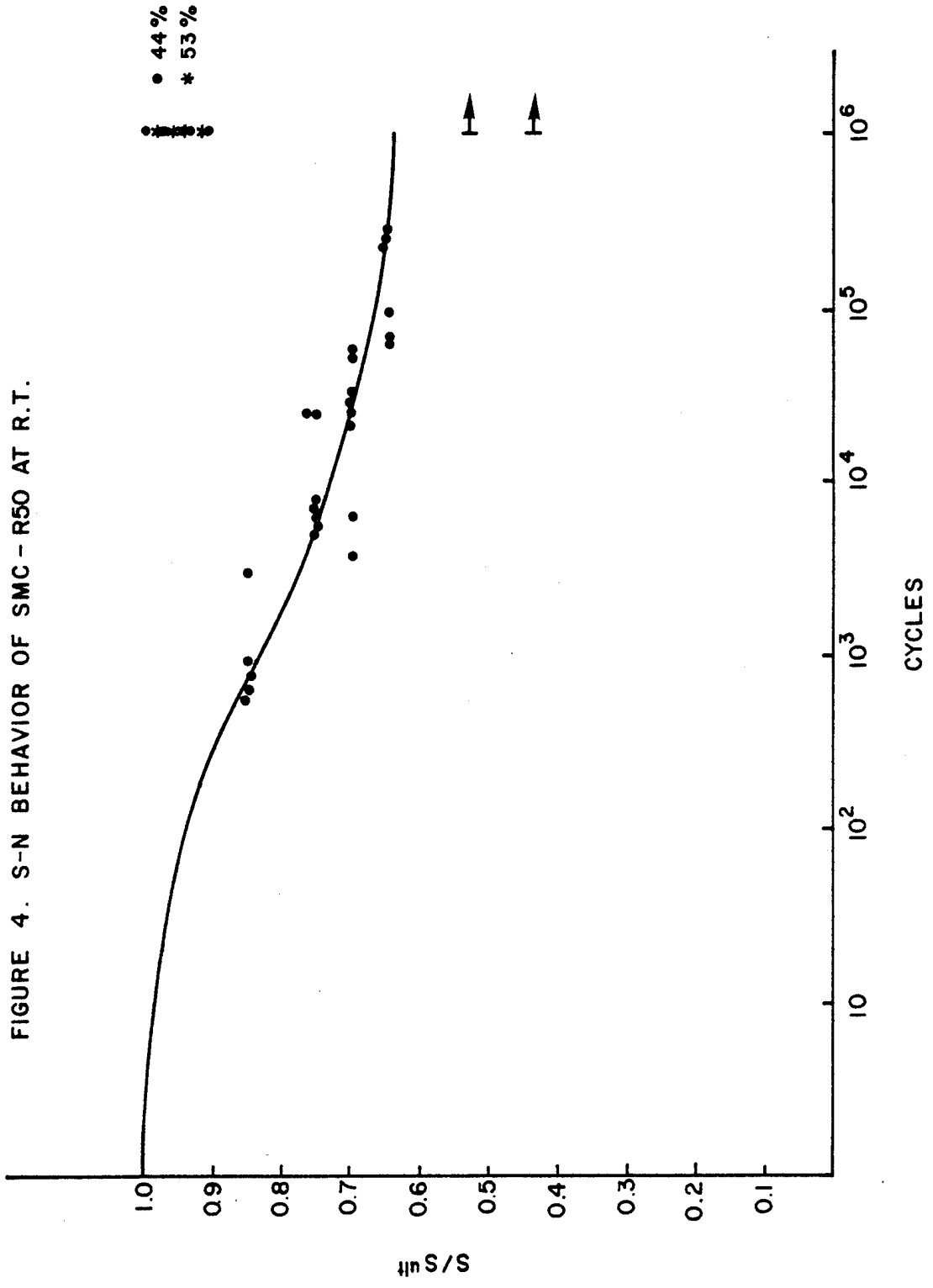

FIGURE 4. S-N BEHAVIOR OF SMC - R50 AT R.T.

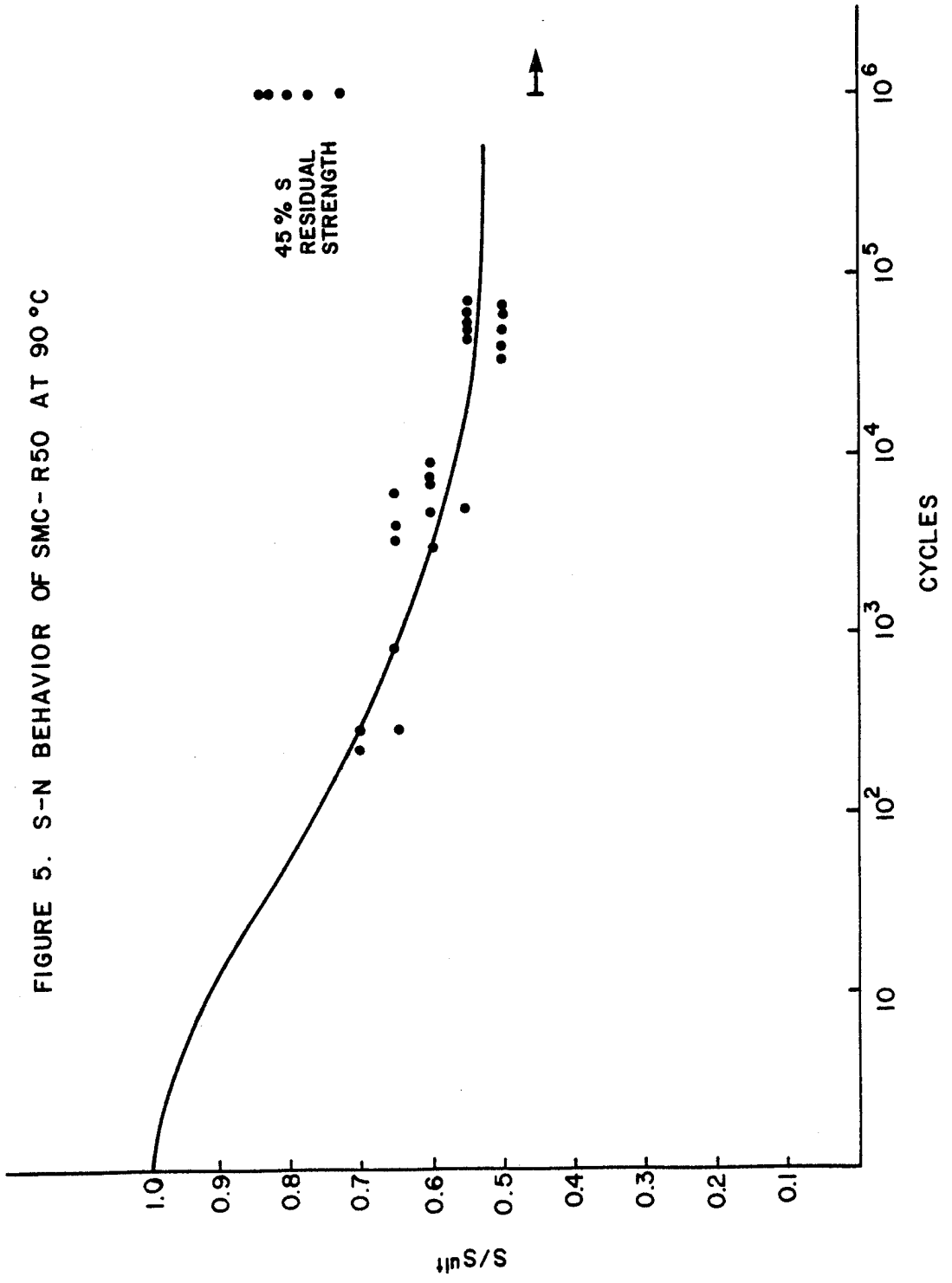

FIGURE 5. S-N BEHAVIOR OF SMC-R50 AT 90 °C

Shear Modulus Characterization

The shear modulus, G_{xz} characterization for untested specimens at 21°C and 90°C is summarized in Table 4. The modulus measured at room temperature varied from 2.3 GPa (0.29 Msi) to 3.0 GPa (0.44 Msi) with a mean value of 2.65 MPa (0.36±0.6 Msi). At 90°C G_{xz} was measured to be 0.83 MPa (0.12 Msi).

Modulus data obtained for the specimens subjected to fatigue was not as extensive as planned. At room temperature specimens were tested at 60 percent of ultimate strength to approximately 50 percent and 90 percent of cycles to failure. The shear modulus G_{xz} measured for these specimens was 2.6 MPa (0.38 Msi) and 2.4 MPa (0.35 Msi), respectively. Since these results are within the scatter band of the untested controls, the modulus appears unchanged with fatigue loadings over 90% of the material's expected fatigue life. A similar data point for the 90°C temperature for a specimen tested to 50 percent of its fatigue life resulted in a modulus of 1.2 MPa (0.18 Msi). This modulus is greater than the average modulus measured for material at 90°C, but is within a reasonable scatter band considering the test method and material variability. Not enough specimens were available to obtain more data points.

TABLE 4

SHEAR MODULUS DATA FOR SMC-R50

Specimen	Temperature (°C)	Span (mm)	G_{xz} (GPa)
3A-6	21	25.4	2.3
4B-12	21	25.4	3.0
3A-6	90	25.4	0.83
4B-12	90	25.4	0.83

Microstructural Studies

Both optical and scanning electron microscope were used to examine the SMC before and after fatigue tests. Figure 6 shows typical microstructure of an untested specimen at 50X magnification. There are distinct strata defining regions where groups of fiber bundles lie in the same plane. The orientation of the fibers appeared to be primarily parallel to the axis of the beam for all sections examined. The region labeled "A" in Fig. 6 is a matrix-rich area or void region filled with mounting epoxy. These regions were typical of all sections examined. An SEM photomicrograph of these matrix rich regions magnified to 320X is shown in Figure 7. The matrix appeared to be riddled with small voids. A specimen which was cycled at an 85 percent S level and failed at 980 cycles as shown in Figures 8a and 8b. The figures show matrix cracking (crazing) in the specimen. These cracks were sparse in this specimen and very few occurances of such cracks were found in the cross sections of other specimens examined. Neither temperature, S level nor number of cycles bore any distinct relationship to the very insignificant amount of matrix or fiber-matrix interface damage observed.

Optical micrographs of the typical cracks in the failed specimens were similar to the one shown in Figure 9. The crack cleavage plane followed the boundary be-

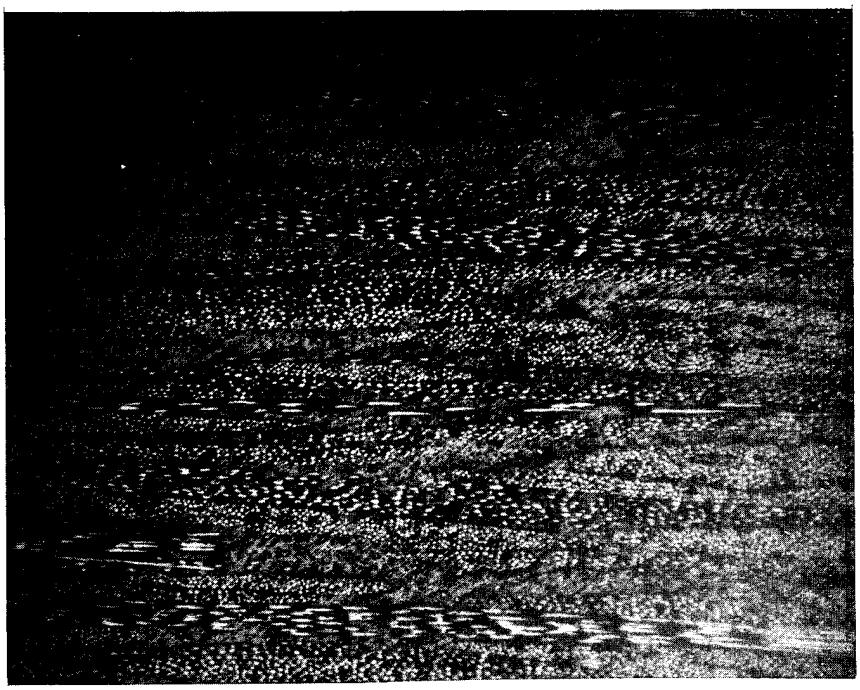

Figure 6. Photomicrograph of cross-section through untested SMC-R50 specimen at 50X magnification

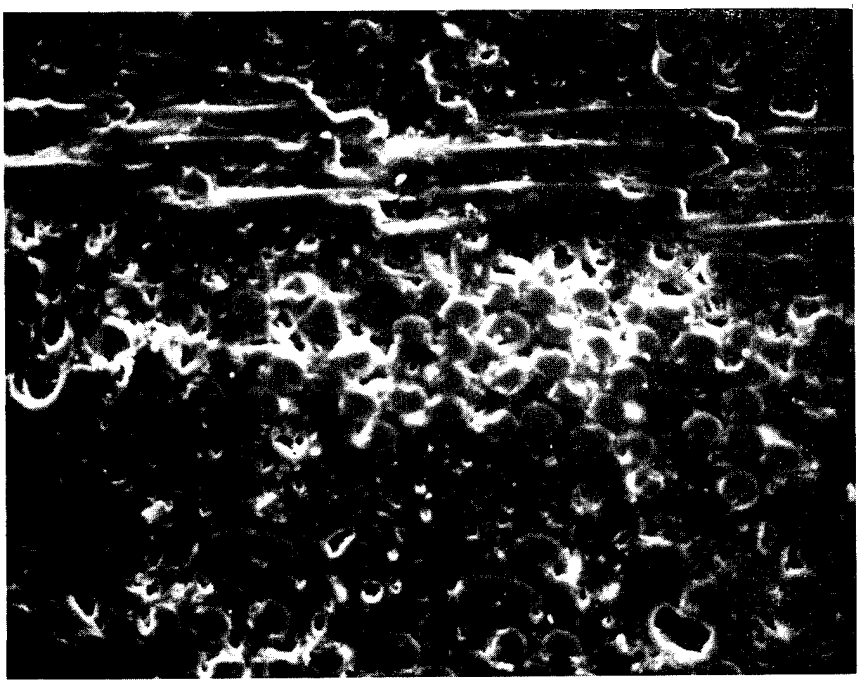

Figure 7. A magnification showing microstructure of an untested SMC-R50 specimen

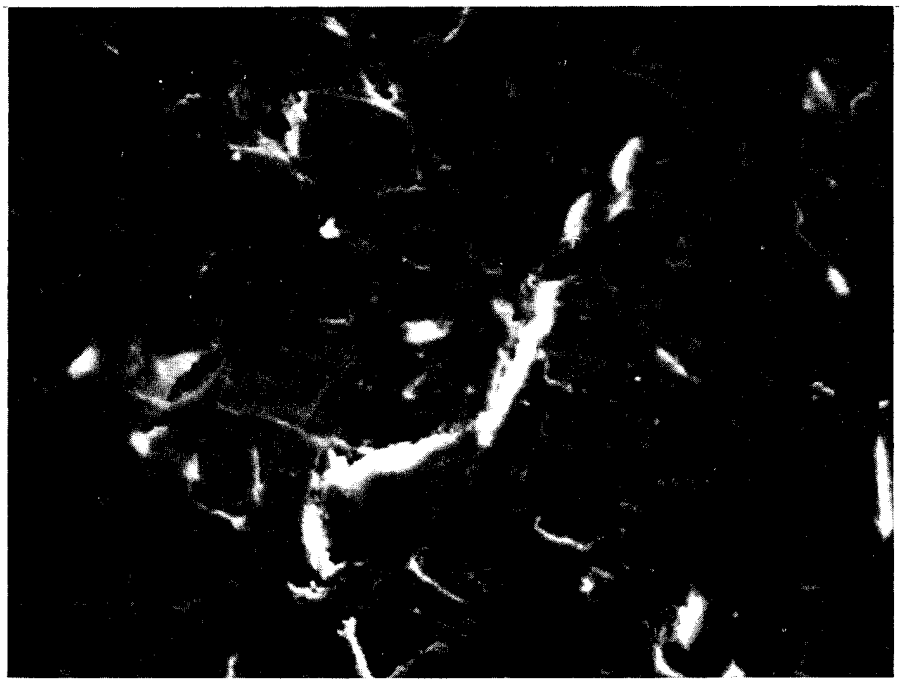

Figure 8a. Matrix crack developed in specimen tested at 85% stress level (640X magnification)

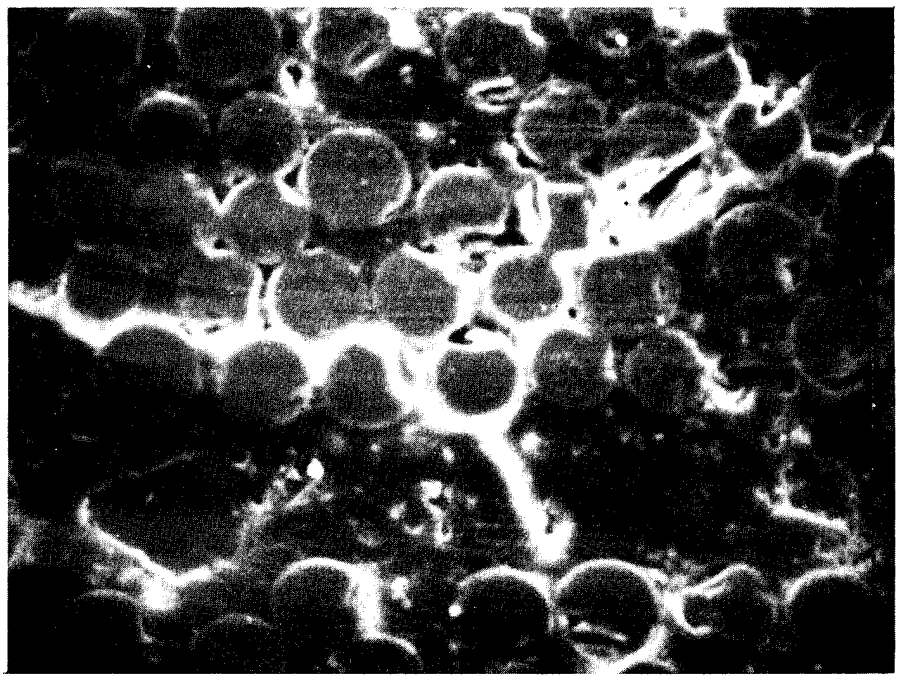

Figure 8b. Example of crack development at the fiber-matrix interfaces in the same specimen

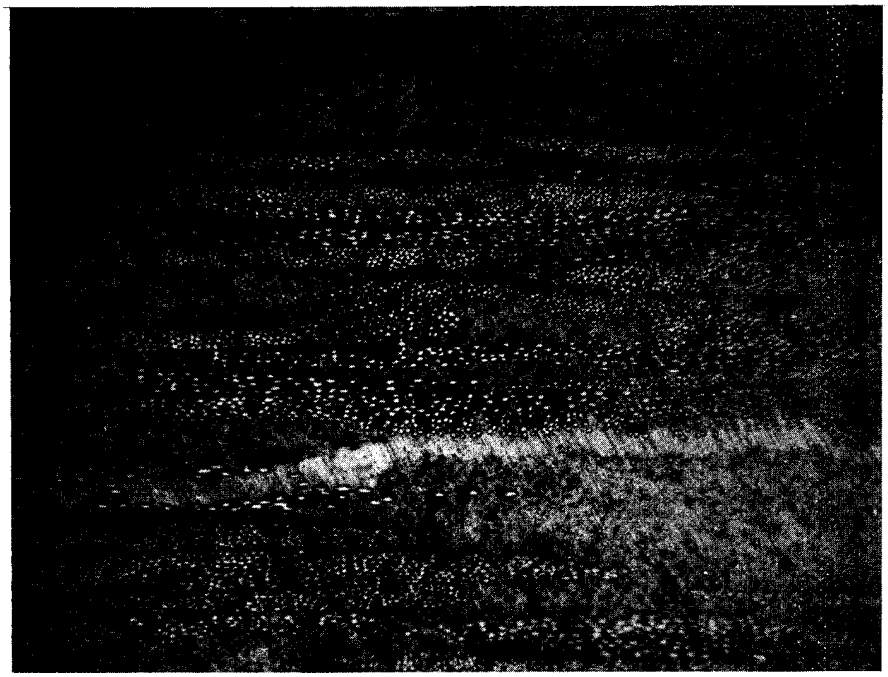

Figure 9. Crack path through specimen failed statically (50X magnification)

tween fiber bundles or propagated through matrix rich areas.

Finite-Element Analysis of Shear Stress at Midplane

In order to determine the shear stress distribution in the thick beam sandwich test coupon used in this test program, a two-dimensional linear, finite-element (F-E) analysis was performed. The material properties given in Table 5 were utilized in the F-E model illustrated in Figure 10.

Specimen symmetry was used in the model design and the boundary conditions are clearly indicated in the figure describing the element mesh. The resulting stress profiles along the midplane are plotted in Figure 11. The normal stress σ_{zz} perpendicular to the beam axis is large at the load introduction and reaction points while dropping to zero between the reaction points and becoming tensile at the free end. The shear stress τ_{xz} is zero at the loading point at the midspan and at the free end. At the quarter span ($x/L = 0.25$) the stress is uniform for approximately 5 mm (0.2 in) then decreases nonlinearly to zero. Figure 12 shows the shear stress distribution through the thickness at portions near the quarter span. It is clear that the beam was virtually in a state of uniform shear stress at the quarter span.

TABLE 5

MATERIAL PROPERTY INPUT DATA
FOR THE FINITE ELEMENT MODEL

Property	SMC-R50	Gr/E
E_m	2.27	20.0
E_s	1.15	1.4
E_t	2.27	1.4
ν_{ns}	.22	.21
ν_{nt}	.31	.31
ν_{st}	.22	.02
G_{ns}	.33	.6

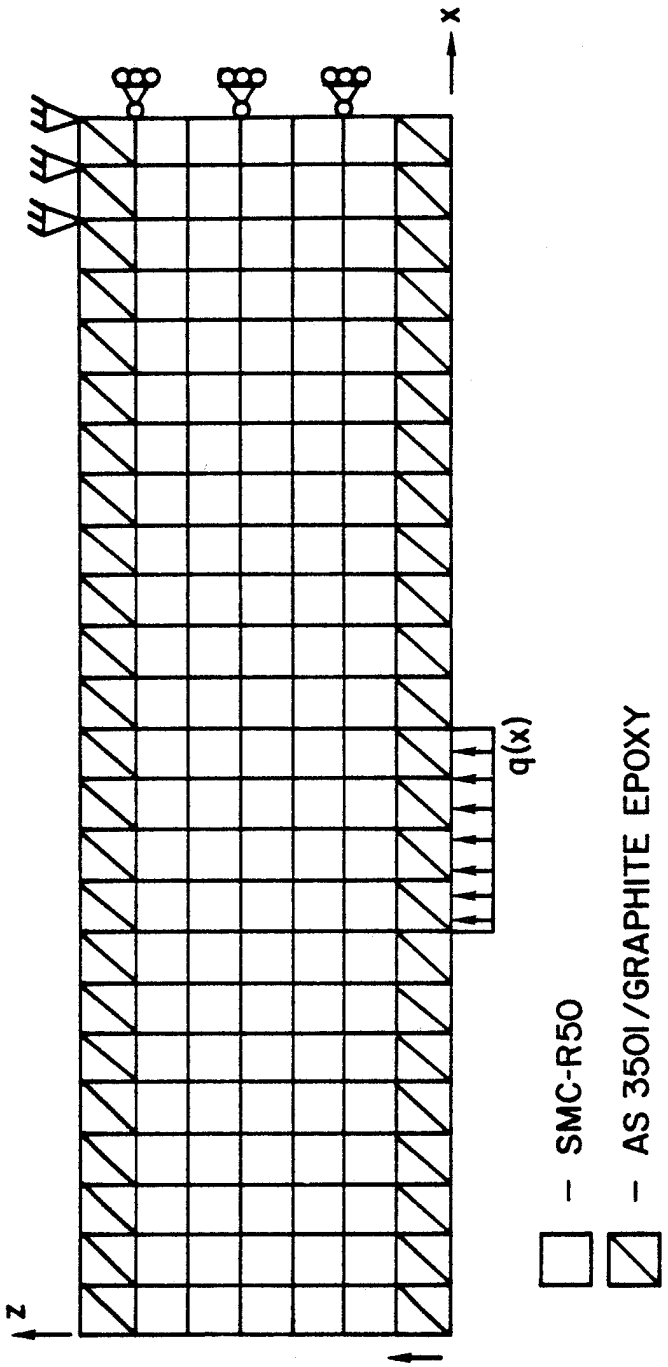

FIGURE 10. FINITE ELEMENT MODEL FOR SANDWICH BEAMS

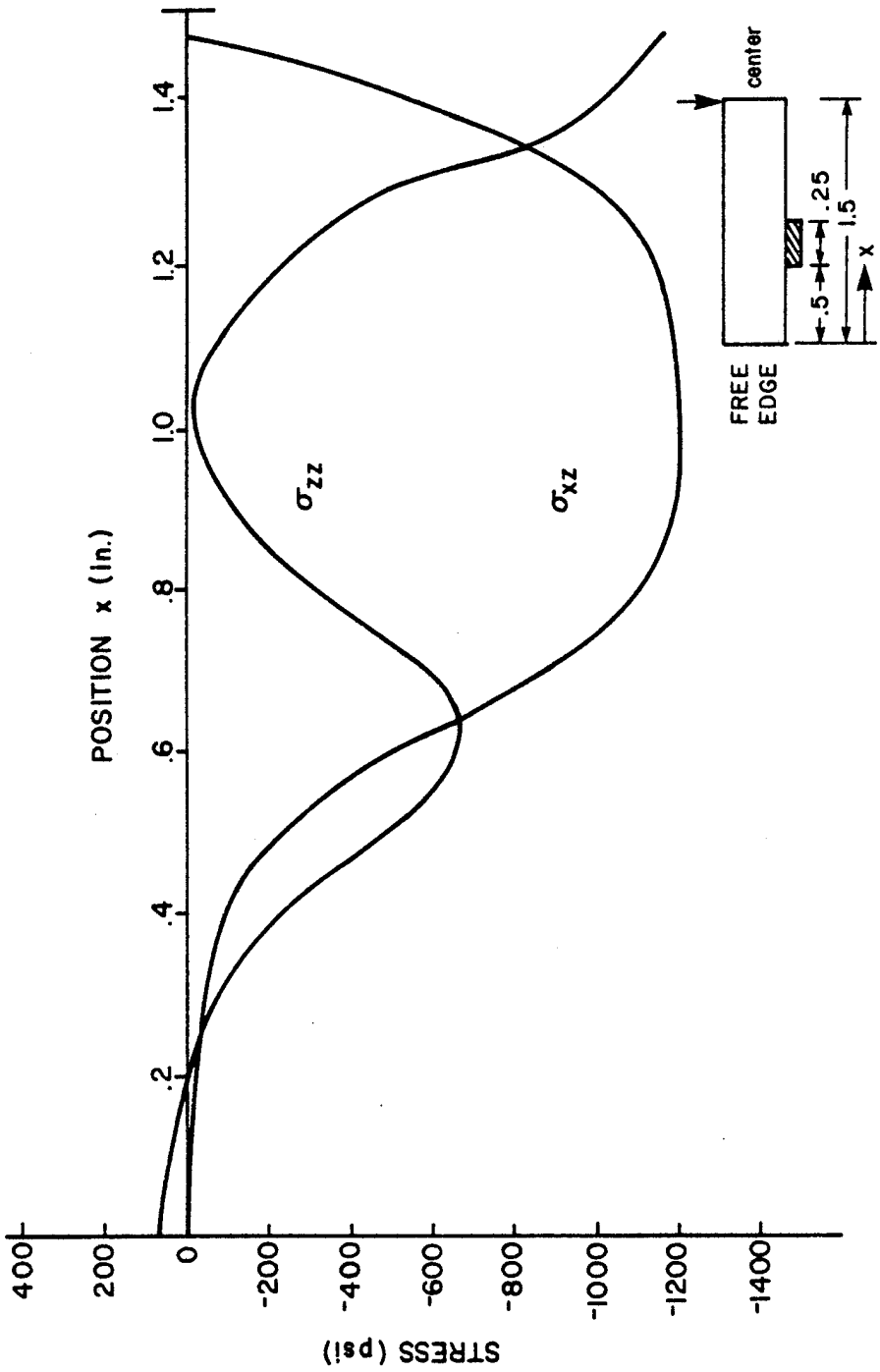

FIGURE. 11. PLOT OF THE STRESSES σ_{xz} AND σ_{zz} ALONG THE HALF-SPAN OF THE BEAM.

FIGURE 12. SHEAR STRESS DISTRIBUTIONS THROUGH THICKNESS OF THE BEAMS.

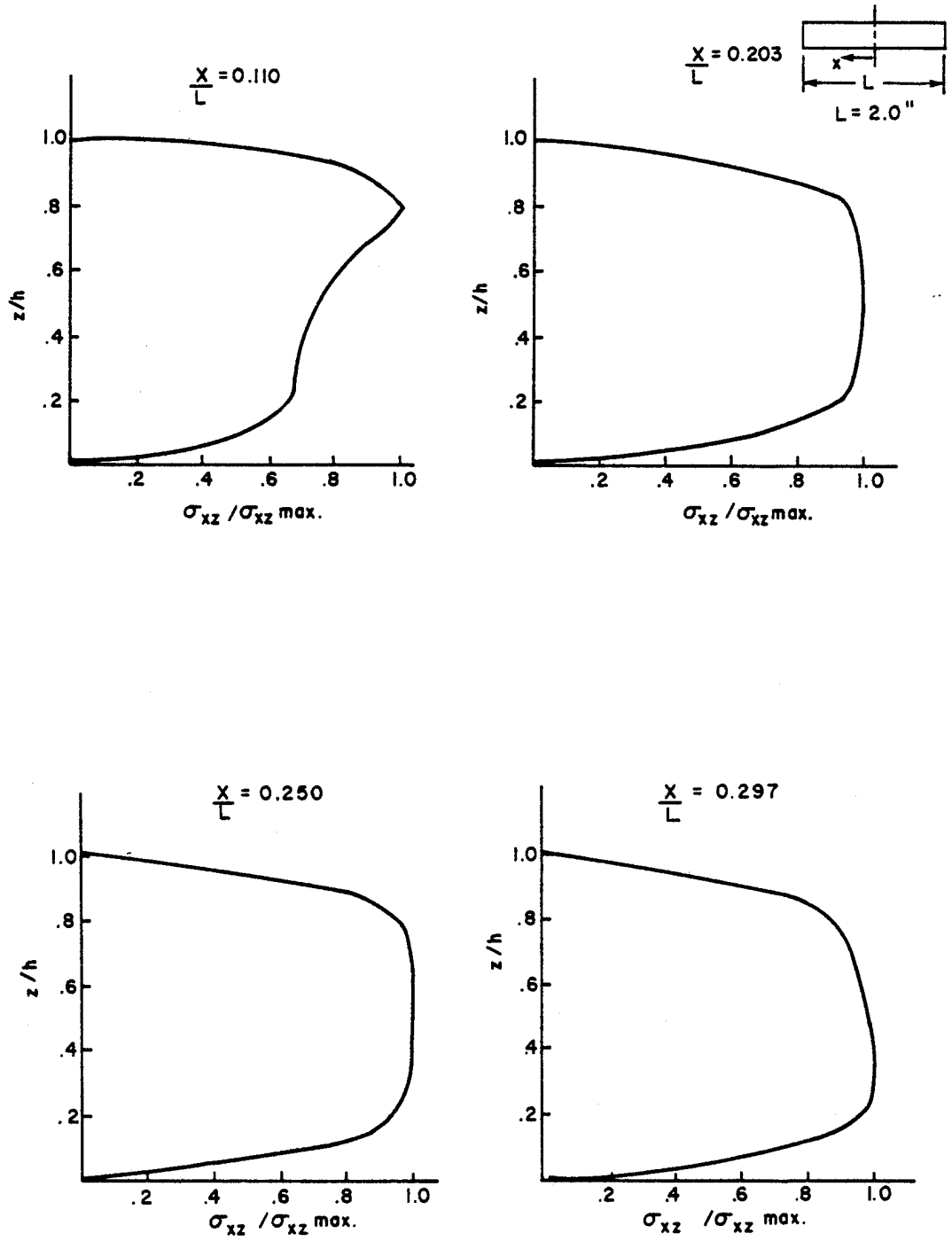

Discussion

Fatigue degradation of composite interlaminar properties is usally attributed to the accumulation of distributed damage in the matrix phase and at the fiber-matrix interface throughout the material. Studies reported in the literature indicate the matrix crazing and failure of the fiber-matrix interface are responsible for the degradation in strength and stiffness of continuous fiber composites subjected to flexural fatigue. The experimental evidence of this study suggests that a different mechanism is playing the key role in the fatigue life of the SMC-R50 material.

The combination of results from three facets of this research suggest that fatigue life in SMC-R50 is primarily controlled by flaw criticality. This implies that failure is caused by damage propagation stemming from an initial flaw. The damage is a localized phenomena associated with the "critical flaw" and results in eventual catastrophic failure. Stress amplitude and the cyclic application of the load serve to initiate and propagate the flaw. Once the damage is initiated the applied stress causes a rapid crack propagation and failure of the specimen. The flaw criticality hypothesis is substantiated by the residual strength results, modulus measurement and microstructural analysis of fatigue damage for the SMC

system studied.

Fatigue life of a material is usually characterized by an S-N curve which shows the relationship between the stress amplitude and number of cycles to failure. The S-N curve is a monotonically decreasing exponential function for most materials which may level out to some constant stress amplitude termed the "endurance limit." At stresses below the endurance limit fatigue failures in the material are not probable. For the normal fatigue mechanism in composites, the residual strength of the material after a specific number of cycles corresponds to the fatigue strength of the material (i.e., the residual strength would fall on the S-N curve which would result in failure at that number of cycles). The results for the SMC-R50 did not follow this behavior. Residual strengths at 21°C for the 53 percent and 44 precent stress levels were greater than 90 percent of the static ultimate strength after 10^6 cycles. Similarly at 90°C for the 45 percent stress level the residual strength after 10^6 cycles was greater than 80 percent of the average static ultimate strength. This evidence suggests that damage accumulation is not occuring and that some other mechanism is responsible for the S-N behavior exhibited at the higher stress levels.

Measurements of the shear modulus G_{xz} after fatigue

at a 60 percent stress level for a number of cycles equivalent to 90 percent of the expected fatigue life of the material showed no decrease in stiffness. This evidence further substantiated the conclusion drawn from the residual strength results that global cumulative damage was not occuring.

Microstructural studies verified the assumption about significant fatigue related damage accumulation for less 10^6 angles in fatigue. No evidence of significant matrix crazing or fiber-matrix interface damage was observed. The examination of fatigue failures showed that the only damage was that which was related to the catastrophic failure sites. Cleavage planes in the failed specimens followed matrix rich regions and planes between the strata defining the fiber bundles. High magnification photomicrographs of these regions reveal large numbers of voids. These voids could serve as crack initiation sites in fatigue. Thus the evidence strongly suggests the hypothesis that the failure mechanism of SMC-R50 is governed by flaw criticality not cumulative damage. Cracks are initiated at some critical flaw inherent in the material which results in a localized rapid crack propagation and subsequent failure. The number of cycles to crack initiation at a specific stress level governs the S-N behavior. After crack initiation the progression to failure is rapid.

CONCLUSIONS

Two important conclusions can be drawn from the fatigue characterization of interlaminar shear properties for SMC-R50 sheet molding compound.

1. The fatigue life of the interlminar shear properties is temerpature-sensitive. S-N behavior showed that at 90°C the endurance limit for ILS strength was about 15 percent lower than at 21°C.

2. The fatigue life of SMC-R50 is primarily controlled by a flaw criticality phenomenon. Failure in interlaminar shear fatigue results from propagation of localized damage initiated at an inherent material flaw as opposed to a distributed damage accumulation throughout the matrix phase and fiber-matrix interface.

REFERENCES

1) Sattar, S. A. and Kellog, D. H., "The Effect of Geometry on the Mode of Failure of Composites in Short Beam Shear Test," Composite Materials: Testing and Design, ASTM STP 460, American Society for Testing and Materials, 1969, pp. 62-71.

2) Kedward, K. T., "On the Short Beam Test Method," Fibre Science and Technology, (5) , 1972, pp. 85-95.

3) Pipes, R. B., Reed, D. L., and Ashton, J. E., "Experimental Investigation of the Interlaminar Shear Properties of Composite Materials," unpublished research, paper presented at the 1972 SESA Spring Meeting, Cleveland, Ohio.

4) Pipes, R. B., "Interlaminar Shear Fatigue Characteristics of Fiber-Reinforced Composite Materials," Composite Materials: Testing and Design, ASTM STP 546, American Society for Testing and Materials, 1974, pp. 419-432.

5) Owen, M. J. and Morris, S., "Some Interlaminar-Shear Fatigue Properties of Carbon-Fiber-Reinforced Plastics," Plastics and Polymers, Vol. 40, No. 148, August 1972, pp. 209-216.

6) Dharin, C. R. H., "Interlaminar Shear Fatigue of Pultruded Graphite Fibre-Polyester Composites," Journal of Materials Science, Vol. 13, No. 6, (1978), pp. 1243-1248.

7) Bevan, L. G., "Axial and Short Beam Shear Fatigue Properties of CFRP Laminates," Composites. Vol. 8, No. 4, Oct 1977, pp. 227-232.

8) Agarwal, B. D. and Joneja, S. K., "Progressive Damage in GFRP under Constant Deflection Flexural Fatigue," Fibre Science and Technology, Vol. 12, No. 5, Sept. 1979, pp. 341-352.

9) Smith, E. W. and Pascoe, K. J., "The Role of Shear Deformation in Fatigue Failure of a Glass Fibre-Reinforced Composite," Composites, Vol. 8, No. 4, Oct 1977, pp. 237-243.